

# Global Precipitation Correction Across a Range of Climates Using CycleGAN

J. McGibbon<sup>1\*</sup>, S. K. Clark<sup>1,2†</sup>, B. Henn<sup>1‡</sup>, A. Kwa<sup>1§</sup>, O. Watt-Meyer<sup>1¶</sup>, W. A. Perkins<sup>1||</sup>, C. S. Bretherton<sup>1\*\*</sup>

<sup>1</sup>Allen Institute for Artificial Intelligence, Seattle, WA, USA  
<sup>2</sup>Geophysical Fluid Dynamics Laboratory, Princeton, NJ, USA

## Key Points:

- A Cycle-generative adversarial network (CycleGAN) can debias precipitation across a range of climate forcings
- The model is able to debias data from intermediate forcings not present in training data
- The model is able to correct tails of the precipitation distribution without the use of quantile mapping

---

\*Contribution: Conceptualization, Investigation, Methodology, Formal analysis, Software, Visualization, Writing - original draft, Writing - review and editing

†Contribution: Data curation, Methodology, Software, Writing - original draft, Writing - review and editing

‡Contribution: Software, Writing - review and editing

§Contribution: Software, Writing - review and editing

¶Contribution: Software, Writing - review and editing

||Contribution: Software, Resources, Writing - review and editing

\*\*Contribution: Project administration, Supervision, Conceptualization, Formal Analysis, Writing - original draft, Writing - review and editing

Corresponding author: Jeremy McGibbon, [mcgibbon@uw.edu](mailto:mcgibbon@uw.edu)

## 14 **Abstract**

15 Accurate precipitation simulations for various climate scenarios are critical for under-  
 16 standing and predicting the impacts of climate change. This study employs a Cycle-generative  
 17 adversarial network (CycleGAN) to improve global 3-hour-average precipitation fields  
 18 predicted by a coarse grid (200 km) atmospheric model across a range of climates, mor-  
 19 phing them to match their statistical properties with reference fine-grid (25 km) simu-  
 20 lations. We evaluate its performance on both the target climates and an independent  
 21 ramped-SST simulation. The translated precipitation fields remove most of the biases  
 22 simulated by the coarse-grid model in the mean precipitation climatology, the cumula-  
 23 tive distribution function of 3-hourly precipitation, and the diurnal cycle of precipita-  
 24 tion over land. These results highlight the potential of CycleGAN as a powerful tool for  
 25 bias correction in climate change simulations, paving the way for more reliable predic-  
 26 tions of precipitation patterns across a wide range of climates.

## 27 **Plain Language Summary**

28 Using CycleGAN, a machine learning technique, we can remove key biases in precipi-  
 29 tation simulated by a fast, coarse-grid atmospheric model. This method morphs maps  
 30 of the output precipitation to match typical characteristics of a slower but more accu-  
 31 rate fine-grid configuration, correcting systematic errors in both long-term average spa-  
 32 tial precipitation patterns and 3-hourly precipitation variations. It retains skill in inter-  
 33 mediate climate states unseen in training, making it a useful tool for climate change sim-  
 34 ulations.

## 35 **1 Introduction**

36 Throughout the history of atmospheric model development, results from fine-grid  
 37 models that resolve important physical processes like cloud and precipitation formation  
 38 or flow over mountain ranges have been used to improve biased climates in coarse-grid  
 39 models that do not. For instance, scientists have used large-eddy simulations as a test-  
 40 bed for calibrating analytic turbulence and cloud parameterizations, e.g. Bogenschutz  
 41 et al. (2010). This process relies heavily on expert knowledge to develop appropriate mod-  
 42 els of sub-grid behaviors, often heavily influenced by analysis of a few archetypical cases.

43 More recently, machine learning (ML) has been used to correct coarse-resolution  
 44 models' behavior across the full range of conditions over historical periods where obser-  
 45 vational analysis is available. For example, Watt-Meyer et al. (2021) trained a correc-  
 46 tive tendency for a 200 km grid atmospheric general circulation model (AGCM) using  
 47 ML based on nudging tendencies towards observational analysis. The ML correction re-  
 48 duced annual-mean precipitation biases by 20%. An ML approach based on reservoir com-  
 49 puting (Arcomano et al., 2023) and ERA5 reanalysis (Hersbach et al., 2020) halved the  
 50 global root mean square bias of annual-mean precipitation in an even coarser (400 km  
 51 grid) AGCM.

52 We require a different strategy when training a model to generalize across future  
 53 climate forcings, as when training with observational analyses one can only learn the cli-  
 54 mate represented by this data. One method is to use finer-grid AGCM simulations as  
 55 training targets. Such simulations are computationally expensive, but they more accu-  
 56 rately simulate societally-important aspects of present-day climate such as means and  
 57 extremes of land surface precipitation and temperature than do coarse-grid AGCMs (Flato  
 58 et al., 2013; Wehner et al., 2010). Because they resolve much more detail of deep con-  
 59 vective storm systems, orography and land surface characteristics, they are less sensi-  
 60 tive to uncertain parameterizations of deep convection and orographic drag, making them  
 61 potentially a more robust simulation tool for generalizing to future climates. S. K. Clark  
 62 et al. (2022) used the same nudging approach as Watt-Meyer et al. (2021) to ML-correct

63 a 200 km model to behave like its 25 km analogue across four climates forced by adding  
 64 specified uniform sea-surface temperature (SST) increments to observed SST patterns.  
 65 They were able to correct spatial patterns of precipitation over land by 10-30% in multi-  
 66 year simulations across all four climates.

67 This bias reduction is encouraging, but to get full advantage from high-fidelity refer-  
 68 ence data, corrective ML should enable both the weather and climate to have much  
 69 reduced bias (much less than 50% of a no-ML baseline simulation) vs. this reference, both  
 70 for means and extremes of salient quantities such as precipitation. Yet fundamental chal-  
 71 lenges persist. This type of hybrid ML, which couples a bias correction model trained  
 72 offline with a pre-existing AGCM, can induce online simulation biases due to feedbacks  
 73 between these two components (Brenowitz et al., 2020). The machine learning goal of  
 74 minimizing prediction error for each sample can lead to difficulties in accurately repre-  
 75 senting small-scale stochastic behaviors such as deep convection, leading e.g. to an in-  
 76 accurate representation of the frequency of extreme precipitation (Kwa et al., 2023).

77 To further reduce bias in the simulated space-time distribution of precipitation vs.  
 78 a reference climatology, we turn to a different form of ML, the Cycle-generative adver-  
 79 sarial network or CycleGAN (Zhu et al., 2017), which is a promising tool for translation  
 80 of image data between two unpaired domains. Unlike the above hybrid ML approaches,  
 81 this is a post-processing approach which cannot easily be analyzed in terms of physical  
 82 process errors in the coarse-grid model, and only corrects selected model fields (precip-  
 83 itation, in our case). In the past, cycle-generative networks have been effectively used  
 84 for offline bias correction, but it has been necessary to augment the cycle-generative net-  
 85 work with quantile mapping to achieve accurate probability distributions of precipita-  
 86 tion (François et al., 2021; Pan et al., 2021; Fulton et al., 2023). These works focused  
 87 on translating one or more model output variables towards an observational analysis over  
 88 a historical period for a subset of the globe, the annual cycle, or both, and each corrected  
 89 daily-mean precipitation.

90 Our work expands on these efforts. We use the original CycleGAN architecture of  
 91 Zhu et al. (2017) to correct the output of the FV3GFS atmospheric model with a C48  
 92 cubed-sphere grid (with approximately 200 km horizontal spacing) to behave like the coars-  
 93 ened output of the same model run on a C384 cubed-sphere grid (25 km spacing). We  
 94 demonstrate the ability to improve both the spatial distribution of annual-mean precip-  
 95 itation and the cumulative distribution function (CDF) of 3-hourly precipitation up to  
 96 the 99.999th percentile across a range of climate forcings, without the need for quantile  
 97 mapping. This method is capable of correcting data at intermediate climate forcings not  
 98 used during model training, enabling its application to climate change simulations.

## 99 2 Dataset

100 We generate all training data using the FV3GFS atmospheric model (Putman &  
 101 Lin, 2007; Harris & Lin, 2013; Zhou et al., 2019) as described in McGibbon et al. (2021),  
 102 run on a cubed-sphere grid with 63 vertical levels. Annually-repeating cycles of sea sur-  
 103 face temperature (SST) and sea ice are defined based on the observational monthly means  
 104 time-averaged from 1982 to 2012 from the  $1/12^\circ$  Real Time Global Sea Surface Temper-  
 105 ature (Thiébaux et al., 2003) and  $0.5^\circ$  Climate Forecast System Reanalysis (Saha et al.,  
 106 2014) datasets, respectively. We perturb the SSTs by adding globally-constant offsets  
 107 of -2 K, 0 K, +2 K, and +4 K to produce four different sets of forcings while maintain-  
 108 ing the present-day annual cycle of sea ice and carbon dioxide concentration, analogous  
 109 to S. K. Clark et al. (2022). We train using simulations with spacing between SST off-  
 110 sets of 2 K out of concern that precipitation may be too different between forcings at  
 111 the larger 4 K spacing used in S. K. Clark et al. (2022) for the trained model to accu-  
 112 rately generalize to intermediate forcings, though this has not been tested.

113 For each of these SST forcings, a simulation was performed at C48 resolution for  
 114 9 years, 1 month. Eight 1 year, 1 month simulations are performed at C384 resolution  
 115 beginning with the C48 model snapshot state 1 year into the C48 run as well as the state  
 116 every year thereafter; the C48 snapshots were converted to C384 initial conditions us-  
 117 ing the `chgres_cube` tool of `UFS_UTILS` (Gayno et al., 2020). For each of these C384 sim-  
 118 ulations, the first month of simulation time is discarded as a model spin-up period. This  
 119 yields 8 years of useful simulation data from each climate, from which we take the first  
 120 5 years as training and the last 3 years as validation data.

121 During these simulations we accumulate and store the 3-hourly mean precipitation  
 122 rate. We use 3-hourly precipitation instead of daily mean to test the ability of the model  
 123 to correct biases in the diurnal cycle. At each output time, the C384 precipitation fields  
 124 are coarsened to the C48 grid by horizontal averaging so that they can be directly com-  
 125 pared with coarse-grid precipitation fields.

126 We also perform “ramping” simulations at both C48 and C384 resolution, which  
 127 begin with a present-day initial condition and three month spin-up period with 0K forc-  
 128 ing, and then enter a period where the forcing is linearly increased from 0K to +2K over  
 129 the course of 4 years. This data is withheld during training and hyperparameter tun-  
 130 ing, and is used for model evaluation only. It tests whether the CycleGAN can skillfully  
 131 interpolate mean and extreme precipitation patterns between climates on which it was  
 132 trained.

### 133 3 Model formulation and training

134 The model architecture in Zhu et al. (2017) is used with minimal modifications to  
 135 allow processing of cubed-sphere data. Specifically, convolution is performed using halo  
 136 updates on the cubed sphere, where missing corners are filled with zero values. This is  
 137 numerically identical to the convolution approach used in Weyn et al. (2020), except that  
 138 data in the corner of each tile domain is set to zero rather than copying and rotating data  
 139 from the polar tile face. We do not find evidence of corner imprinting despite this choice.

140 The performance of this model is improved by concatenating spatiotemporal ge-  
 141 ometric features to the input of the generator and discriminator models. These features  
 142 are the  $x$ ,  $y$ , and  $z$  positions of each grid cell on a stationary unit sphere in 3-dimensional  
 143 Euclidean space (spatial features), as well as the  $x$  and  $y$  positions of each grid cell on  
 144 a unit sphere in Euclidean space as it rotates with a period of one rotation per day (time  
 145 features). These time features can also be thought of as the  $x$  and  $y$  positions of an hour  
 146 hand on a 24-hour clock indicating the local time, multiplied by  $\cos(\text{latitude})$  to avoid  
 147 discontinuity at the poles. These are used only as inputs of these models, and are not  
 148 output by the generators. The discriminator is given identical geometric features to the  
 149 generator which produced the image being evaluated.

150 The training dataset includes 58400 3-hourly global snapshots, split evenly across  
 151 the four climate forcings. Each epoch, we randomly sample 40000 snapshots with replace-  
 152 ment, training with a batch size of 1. This data only contains two-dimensional cubed-  
 153 sphere surface precipitation rate along with a UTC time, which is used to generate the  
 154 spatiotemporal geometric features.

155 Notably, the climate forcing itself is absent from the training data, as we were able  
 156 to achieve excellent bias correction without it. When we included the SST perturbation  
 157 as input context, as was done for diurnal features, several performance metrics worsened  
 158 without any clear improvements (compare red vs. steel-blue colors in Figures S2 and S3).

159 The model was trained with an exponential learning rate decay. Starting with a  
 160 high learning rate and eventually reducing it further in training is a widely used tech-  
 161 nique in machine learning (Li et al., 2019). The best results shown here were achieved

162 with an initial learning rate of  $10^{-4}$  and a decay factor of 0.63 (a tenfold decrease ev-  
 163 ery 5 epochs). Training converged (in terms of our precipitation bias metrics) by epoch  
 164 14 and was run for 16 epochs (Figure S1).

165 Otherwise, the hyperparameters are the same as in the 6-layer network of Zhu et  
 166 al. (2017), but with twice as many filters in the generator and discriminator. We did not  
 167 attempt to tune the number of layers, activation functions, or choice of optimizer, and  
 168 we found that increasing the number of filters beyond the value used did not im-  
 169 prove the model.

## 170 4 Results

171 Figure 1 shows the behavior of the generative model on a single sample, taken from  
 172 the ramping simulation in a climate state distinct from any in the CycleGAN training  
 173 dataset. We are most concerned with the translation of C48 data into C384 (ML) data  
 174 (upper left vs. upper right panels), but it is also illuminating to see the inverse gener-  
 175 ation from C384 to C48 (ML) (lower left vs. upper right panels). The model introduces  
 176 finer scale features when translating into the C384 domain, especially in lightly precip-  
 177 itating marine boundary layer cloud regimes. It strengthens precipitation over land, in-  
 178 troducing precipitation into areas which have none in the C48 input, for example over  
 179 the South American continent.

180 The translation substantially improves the mean precipitation climatology vs. C48  
 181 simulations for all four SST offsets, as shown in Figure 2, with metrics reported in Fig-  
 182 ure 3. Here and throughout this analysis, time-mean statistics for fixed-SST simulations  
 183 such as for the 0K climate are computed on the 3 years of validation data. Statistics for  
 184 the ramping climate are computed on years 2 and 3 of the 4-year simulation linearly ramp-  
 185 ing from 0K to plus-2K forcings, to highlight the range of SST offsets that are further  
 186 from the fixed-SST training data and hence provide a more rigorous out-of-sample test.  
 187 The bias reductions seen in the ramping simulation are comparable to those in the tar-  
 188 get climates; the bias of mean precipitation averaged over all land is reduced over 85%,  
 189 and the standard deviation of the geographic pattern of time-mean bias is reduced over  
 190 75% to values around 0.5 mm/d. A significant portion of the biases in each target cli-  
 191 mate is explained by differences in precipitation between the validation and training datasets,  
 192 as shown by the “train” bars. Thus, we anticipate further bias reduction with larger train-  
 193 ing and validation datasets.

194 Both the 0 K and ramping simulations have smaller precipitation pattern biases  
 195 than reported for a current-climate case by Arcomano et al. (2023). They reported that  
 196 their hybrid reservoir computing ML reduced the standard deviation of precipitation pat-  
 197 tern bias nearly 50% from 1.2 mm/d in their no-ML baseline model to a value of 0.63 mm/d.  
 198 Our mean precipitation biases also much smaller than the bias shown in Figure 1 of Fulton  
 199 et al. (2023) for the South Asian monsoon region. A direct comparison with François et  
 200 al. (2021) and Pan et al. (2021) is difficult because they considered France and the con-  
 201 tinental United States, respectively, both of which have much smaller biases than the rest  
 202 of the globe in our model.

203 Figure 4 shows that the translated data has a 3-hourly probability distribution and  
 204 a diurnal cycle of land precipitation that much more closely match the C384 reference  
 205 data across all climates, including the ramping simulation. We might expect the Cycle-  
 206 GAN to struggle to represent extreme precipitation events and their sensitivity to cli-  
 207 mate forcing because they appear infrequently in the training data. Nevertheless, the  
 208 58400 precipitation fields, each containing 13824 atmospheric column, comprise almost  
 209  $10^9$  atmospheric columns, perhaps enough to learn how to translate even highly unusual  
 210 precipitation events. Indeed, the CycleGAN improves the accuracy of the CDF of pre-  
 211 cipitation up to the 99.999th percentile. Only at the 99.9999th percentile and only for

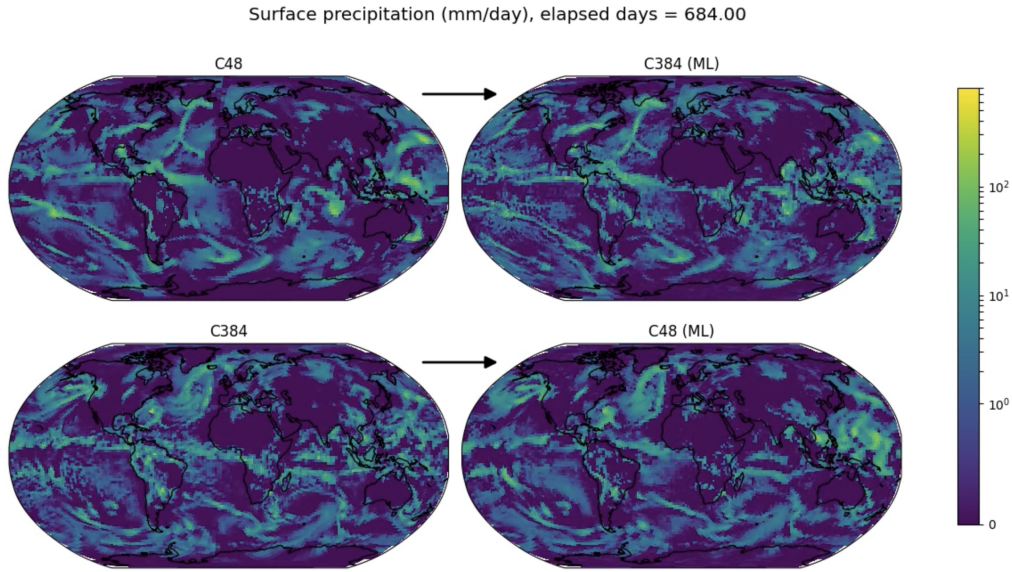


**Figure 1.** Inputs and outputs of the CycleGAN for one timestep during the ramping simulation. Precipitation data on the left was used as input to generate precipitation data on the right. Snapshot was selected to illustrate a common feature, significantly stronger precipitation over South America in C384 (replicated by the GAN) than in C48. All snapshots for this simulation can be viewed in the supplementary data (Movie S1).

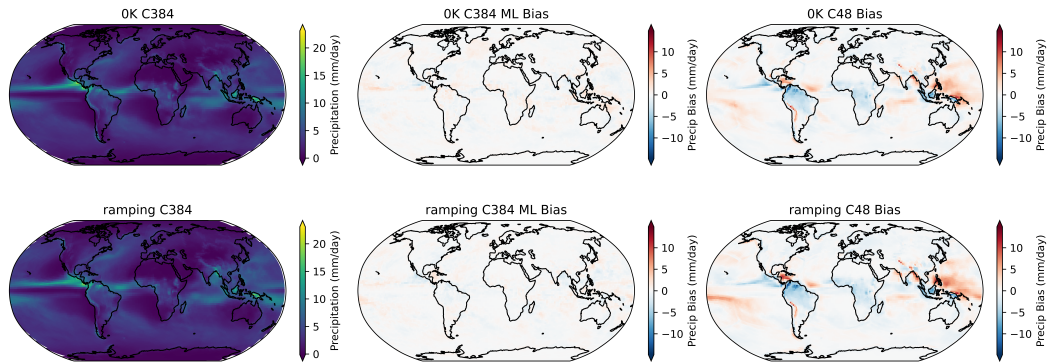


**Figure 2.** Annual-mean precipitation from C384 reference run (left column) and precipitation biases from the C48 simulation (right column) and from the GAN applied to this C48 simulation (C384 ML). Bias values are differences from the C384 reference.

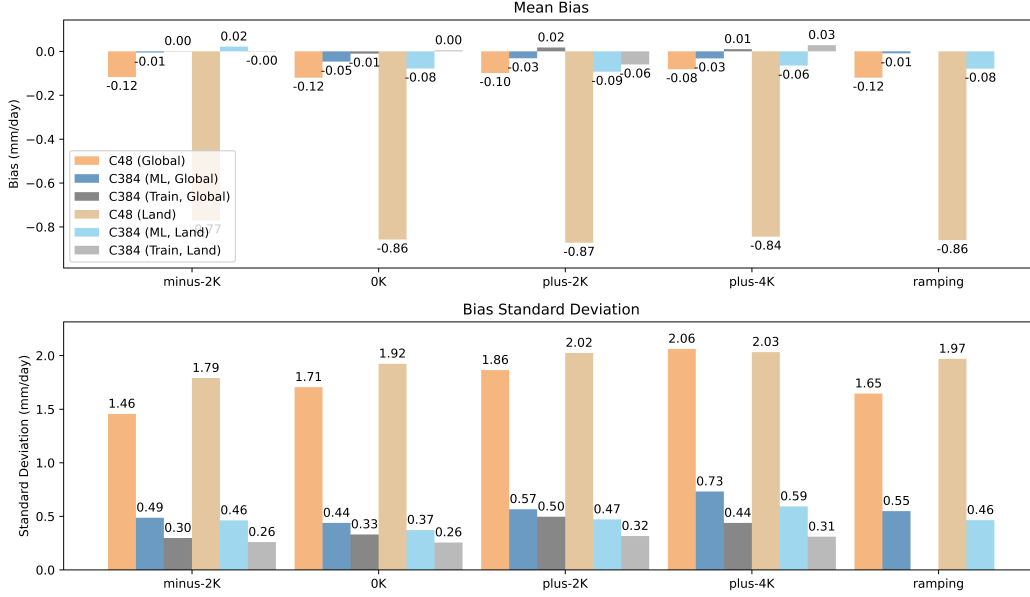


**Figure 3.** Metrics of time-average precipitation bias against validation and testing data. Mean bias refers to the area-weighted horizontal mean bias across all samples, or over land samples only. Bias standard deviation refers to the square root of the area-weighted mean square bias, averaged over the horizontal either globally or over land samples only. These statistics are derived from bias maps as shown in Figure 2. “Train” indicates the comparison of the training data itself against the validation data. Training data is not available for the ramping simulation.

212 the -2 K forcing, the CycleGAN slightly increases the error over the input C48 reference  
 213 data. Surprisingly, the distribution of ML outputs is, if anything, over-dispersive in the  
 214 tails. The shape of the diurnal cycle of precipitation over land is also improved across  
 215 all climate forcings, with a stronger trough and sharper increase in precipitation from  
 216 6:00 to 15:00 local solar time, and more sustained precipitation through the 21:00-24:00  
 217 bin.

218 Here, the diurnal cycle over land was computed by determining the local solar time  
 219 in each land-based grid cell for each sample based on its longitude, and then binning the  
 220 data across local time before taking an area-weighted mean.

## 221 5 Sensitivity Studies

222 This section describes sensitivity studies that help motivate some of our model de-  
 223 sign choices. We initially trained the CycleGAN model with less data, but found the global  
 224 maps of time-averaged precipitation vary significantly from year to year, resulting in sig-  
 225 nificant biases in the trained model as a result of under-sampling the long-term climate.  
 226 When we train the model using only the first year of data from each climate and eval-  
 227 uate on the same 3 years of validation data, the model has significantly worse time-mean  
 228 biases (Figure S2, compare light purple bar to darker blue bar), and does a significantly  
 229 worse job predicting the output CDFs, over-predicting the extremes of each climate’s pre-  
 230 cipitation distribution (Figure S3).

231 Adding spatiotemporal features defining the diurnal cycle as context to the input  
 232 of the generator and discriminator was crucial for correcting the shape of the mean di-

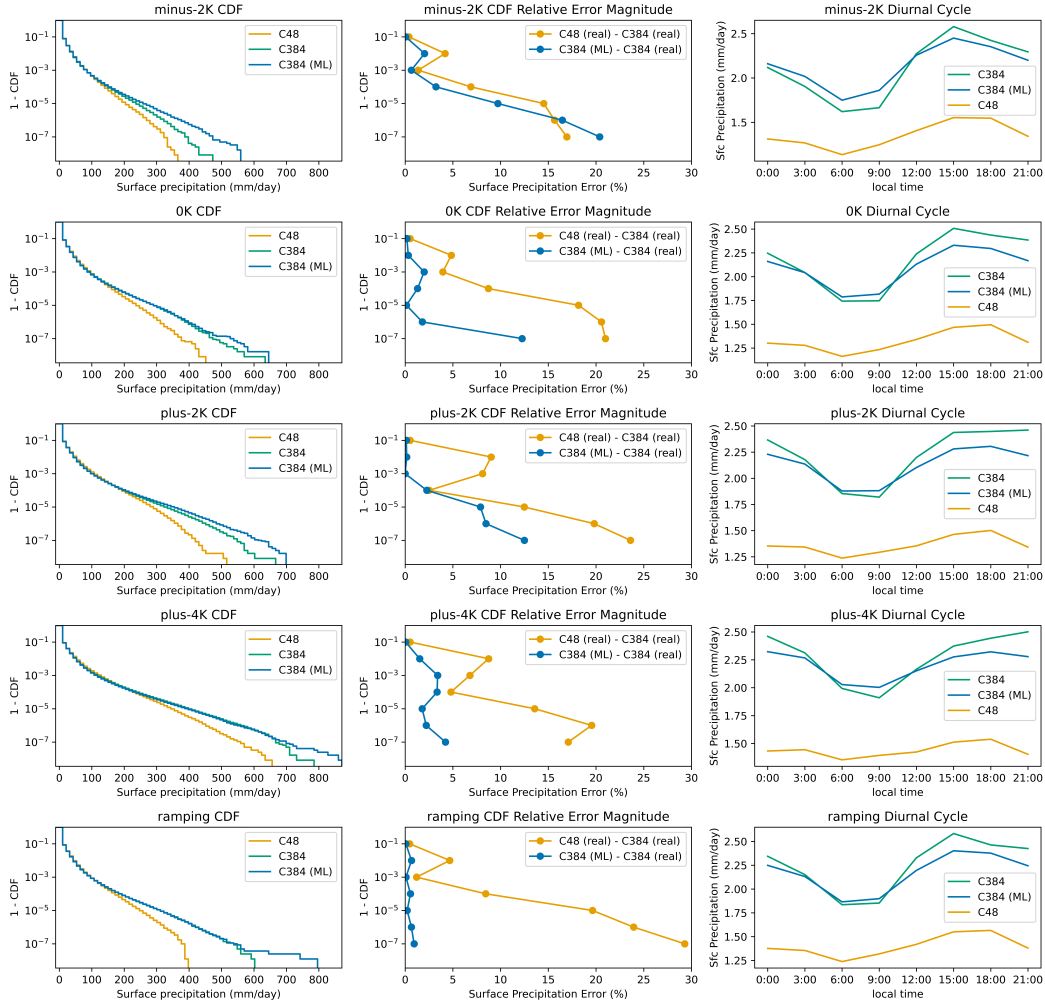


**Figure 4.** CDF metrics and diurnal cycle of precipitation over land for the reference C384 run, the C48 simulation, and the CycleGAN applied to the C48 output (C384 ML). The left column shows the CDF of precipitation for each climate. The center column shows the relative magnitude of errors of the values of the C48 and CycleGAN CDFs in the first column across a range of percentiles, computed as a percentage of the C384 (real) value. The right column shows the diurnal cycle of precipitation over land, with the  $x$ -axis indicating the starting local time of the 3-hour bin.

233 unal cycle of precipitation over land. Without these features, the land diurnal cycle of  
 234 the C384 (ML) output data is significantly improved because we have corrected the cor-  
 235 rect mean and variance, though the shape of the cycle (light green and light blue) is more  
 236 similar to the C48 values (orange). Surprisingly, the inclusion of these features has lit-  
 237 tle impact on the standard deviation of the geographically-resolved time-mean bias (Fig-  
 238 ure S2).

239 In Zhu et al. (2017), an identity loss was included for certain translation tasks to  
 240 avoid unnecessary modification of the color scheme during translation. We find remov-  
 241 ing this identity loss generally degrades model performance. It leads to increased pat-  
 242 tern bias and land-mean bias in precipitation (Figure S2) and has a neutral effect on the  
 243 CDF and land diurnal cycle (Figure S3).

## 244 6 Discussion

245 Unlike previous works using cycle-generative architectures to bias-correct precip-  
 246 itation (François et al., 2021; Pan et al., 2021; Fulton et al., 2023), we could match the  
 247 PDF of 3-hourly precipitation without quantile mapping. Pan et al. (2021) claimed that  
 248 quantile mapping is needed because “GANs are trained to produce individual trust-worthy  
 249 samples, not accurate probability distribution estimations”, due e.g. to mode collapse  
 250 (Bau et al., 2019), despite the claim in Goodfellow et al. (2014) that their training Al-  
 251 gorithm 1 is designed to “converge to a good estimator of [the probability distribution  
 252 of the data], if given enough capacity and training time”.

253 Many methodological differences might explain why we were able to better sim-  
 254 ulate the probability of extreme precipitation events without quantile mapping. We cor-  
 255 rect only precipitation, without using other model output fields as dynamical constraints  
 256 (Pan et al., 2021) or additional fields to be corrected (François et al., 2021; Fulton et al.,  
 257 2023). Fully sampling the variability and covariability within more fields requires sig-  
 258 nificantly more data, owing to the curse of dimensionality. In addition, our model is trained  
 259 on more data than the previous studies. We used 58,400 timesteps each with 13,824 grid-  
 260 cells, resulting in 807M precipitation samples, while François et al. (2021); Pan et al. (2021)  
 261 and Fulton et al. (2023) used 7.42M, 247M, and 40.6M samples respectively. The char-  
 262 acter of the corrections is different, in particular because of the use of 3-hourly versus  
 263 daily data and the use of global data instead of limited regions. Our training method-  
 264 ology also differs in the introduction of a learning rate schedule, which could play a role,  
 265 and Fulton et al. (2023) used the UNIT architecture (Liu et al., 2017) as opposed to Cy-  
 266 cleGAN.

267 While this CycleGAN significantly improves the climate of individual samples from  
 268 a spun-up C48 model state, it should not be used to correct weather simulations run at  
 269 C48 which are initialized from a coarsened C384 state. We trained the CycleGAN only  
 270 on samples which are far into a C48 simulation, whose climate contains more significant  
 271 biases than a hypothetical dataset containing samples from the first week of a C48 sim-  
 272 ulation initialized from coarsened C384 data. One could remove this input bias effect by  
 273 training a CycleGAN model to correct model biases at one particular forecast lead time,  
 274 and using coarse and fine-grid examples at that particular lead time. One could also train  
 275 a conditional CycleGAN with forecast lead time as a model input capable of correcting  
 276 a variety of lead times, similar to what was done in this work for time-of-day.

## 277 7 Conclusions

278 We found that CycleGAN with little modification can accurately translate 3-hourly  
 279 precipitation simulated by a 200 km grid global atmospheric model across a range of cli-  
 280 mate forcing to have similar statistics as output from a reference fine-grid 25 km model,  
 281 as measured by its time-mean geographically-resolved pattern, its CDF and its mean di-

282 urnal cycle over land. These biases are much reduced compared to previous online cor-  
 283 rection approaches, but because CycleGAN is a post-processing approach, this comes at  
 284 the expense of interpretability. The CycleGAN generalizes well to a ramped-SST sim-  
 285 ulation with intermediate forcings not present in the training dataset. With a small set  
 286 of expensive fine-grid simulations, the CycleGAN can thus quickly debias precipitation  
 287 fields predicted by a fast coarse-grid model across a broad range of climates.

## 288 8 Open Research

289 The code used to train and evaluate the machine learning models and produce the  
 290 figures in this study is available on Zenodo via <https://doi.org/10.5281/zenodo.8070950>  
 291 with MIT and BSD licenses (Brenowitz et al., 2023). The coarse-resolution and coars-  
 292 ened high-resolution model output used for training, validation, and testing are avail-  
 293 able on Zenodo via <https://doi.org/10.5281/zenodo.8070973> with a Creative Commons  
 294 Attribution 4.0 International License (S. Clark et al., 2023). Figures were made with Mat-  
 295 plotlib version 3.7.1 (Caswell et al., 2023), available under the matplotlib license at <https://matplotlib.org/>.  
 296 Our machine learning code uses Pytorch version 1.12.1 (Paszke et al., 2019), available  
 297 under a BSD-3 license at <https://pytorch.org/>.

## 298 Acknowledgments

299 We thank the Allen Institute for Artificial Intelligence for supporting this work and NOAA-  
 300 GFDL for providing access to the Gaea computing system used to produce the data on  
 301 which our model is trained and evaluated. We thank Jun-Yan Zhu for making publicly  
 302 available a high-quality PyTorch implementation of the CycleGAN model. We used GPT-  
 303 4 to help create a first draft of the Abstract and Plain Language Summary of this manuscript,  
 304 which were then significantly revised to correct details.

## 305 References

- 306 Arcomano, T., Szunyogh, I., Wikner, A., Hunt, B. R., & Ott, E. (2023). A hybrid  
 307 atmospheric model incorporating machine learning can capture dynamical  
 308 processes not captured by its physics-based component. *Geophysical Research*  
 309 *Letters*, 50(8), e2022GL102649. doi: <https://doi.org/10.1029/2022GL102649>
- 310 Bau, D., Zhu, J., Wulff, J., Peebles, W. S., Strobelt, H., Zhou, B., & Torralba, A.  
 311 (2019). Seeing what a GAN cannot generate. *CoRR*, abs/1910.11626. doi:  
 312 <https://doi.org/10.48550/arXiv.1910.11626>
- 313 Bogenschutz, P. A., Krueger, S. K., & Khairoutdinov, M. (2010). Assumed prob-  
 314 ability density functions for shallow and deep convection. *Journal of Advances*  
 315 *in Modeling Earth Systems*, 2(4). doi: <https://doi.org/10.3894/JAMES.2010.2>  
 316 .10
- 317 Brenowitz, N. D., Henn, B., McGibbon, J., Clark, S. K., Kwa, A., Perkins, W. A.,  
 318 ... Bretherton, C. S. (2020). *Machine learning climate model dynam-*  
 319 *ics: Offline versus online performance.* doi: <https://doi.org/10.48550/>  
 320 [arXiv.2011.03081](https://arxiv.org/abs/2011.03081)
- 321 Brenowitz, N. D., Kwa, A., Perkins, W. A., Henn, B., McGibbon, J., Clark, S., ...  
 322 Nabizadeh, E. (2023, June). *ai2cm/fv3net: Commit used for CycleGAN initial*  
 323 *submission.* Zenodo [Software]. doi: <https://doi.org/10.5281/zenodo.8070950>
- 324 Caswell, T. A., Lee, A., de Andrade, E. S., Droettboom, M., Hoffmann, T., Klymak,  
 325 J., ... Moad, C. (2023, March). *matplotlib/matplotlib: Rel: v3.7.1.* Zenodo  
 326 [Software]. doi: <https://doi.org/10.5281/zenodo.7697899>
- 327 Clark, S., McGibbon, J., & Bretherton, C. (2023, June). *Data for "Global Pre-*  
 328 *cipitation Correction Across a Range of Climates Using CycleGAN".* Zenodo  
 329 [Dataset]. doi: <https://doi.org/10.5281/zenodo.8070973>
- 330 Clark, S. K., Brenowitz, N. D., Henn, B., Kwa, A., McGibbon, J., Perkins, W. A.,

- 331 ... Harris, L. M. (2022). Correcting a 200 km resolution climate model in  
 332 multiple climates by machine learning from 25 km resolution simulations.  
 333 *Journal of Advances in Modeling Earth Systems*, 14(9), e2022MS003219. doi:  
 334 <https://doi.org/10.1029/2022MS003219>
- 335 Flato, G., Marotzke, J., Abiodun, B., Braconnot, P., Chou, S., Collins, W., ...  
 336 Rummukainen, M. (2013). Evaluation of climate models. In T. Stocker  
 337 et al. (Eds.), *Climate change 2013: The physical science basis. contribution*  
 338 *of working group i to the fifth assessment report of the intergovernmental*  
 339 *panel on climate change* (p. 741–866). Cambridge, United Kingdom and New  
 340 York, NY, USA: Cambridge University Press. doi: [https://doi.org/10.1017/](https://doi.org/10.1017/CBO9781107415324.020)  
 341 [CBO9781107415324.020](https://doi.org/10.1017/CBO9781107415324.020)
- 342 François, B., Thao, S., & Vrac, M. (2021, July). Adjusting spatial dependence of  
 343 climate model outputs with cycle-consistent adversarial networks. *Climate Dy-*  
 344 *namics*, 57(11-12), 3323–3353. doi: <https://doi.org/10.1007/s00382-021-05869>  
 345 -8
- 346 Fulton, D. J., Clarke, B. J., & Hegerl, G. C. (2023). Bias correcting climate model  
 347 simulations using unpaired image-to-image translation networks. *Artificial In-*  
 348 *telligence for the Earth Systems*, 1 - 56. doi: <https://doi.org/10.1175/AIES-D>  
 349 -22-0031.1
- 350 Gayno, G., Beck, J., Reames, L., programmer, G., Wright, D., Hu, M., ... Ger-  
 351 heiser, K. (2020, August). *UFS.UTILS*. Unified Forecast System (UFS).
- 352 Goodfellow, I. J., Pouget-Abadie, J., Mirza, M., Xu, B., Warde-Farley, D.,  
 353 Ozair, S., ... Bengio, Y. (2014). *Generative adversarial networks*. doi:  
 354 <https://doi.org/10.48550/arXiv.1406.2661>
- 355 Harris, L. M., & Lin, S.-J. (2013). A two-way nested global-regional dynamical core  
 356 on the cubed-sphere grid. *Monthly Weather Review*, 141(1), 283 - 306. doi:  
 357 <https://doi.org/10.1175/MWR-D-11-00201.1>
- 358 Hersbach, H., Bell, B., Berrisford, P., Hirahara, S., Horányi, A., Muñoz-Sabater,  
 359 J., ... Thépaut, J.-N. (2020). The era5 global reanalysis. *Quarterly*  
 360 *Journal of the Royal Meteorological Society*, 146(730), 1999-2049. doi:  
 361 <https://doi.org/10.1002/qj.3803>
- 362 Kwa, A., Clark, S. K., Henn, B., Brenowitz, N. D., McGibbon, J., Watt-Meyer, O.,  
 363 ... Bretherton, C. S. (2023). Machine-learned climate model corrections  
 364 from a global storm-resolving model: Performance across the annual cycle.  
 365 *Journal of Advances in Modeling Earth Systems*, 15(5), e2022MS003400. doi:  
 366 <https://doi.org/10.1029/2022MS003400>
- 367 Li, Y., Wei, C., & Ma, T. (2019). Towards explaining the regularization effect of  
 368 initial large learning rate in training neural networks. *CoRR, abs/1907.04595*.  
 369 doi: <https://doi.org/10.48550/arXiv.1907.04595>
- 370 Liu, M., Breuel, T. M., & Kautz, J. (2017). Unsupervised image-to-image transla-  
 371 tion networks. *CoRR, abs/1703.00848*. doi: <https://doi.org/10.48550/arXiv>  
 372 [.1703.00848](https://doi.org/10.48550/arXiv.1703.00848)
- 373 McGibbon, J., Brenowitz, N. D., Cheeseman, M., Clark, S. K., Dahm, J. P. S.,  
 374 Davis, E. C., ... Fuhrer, O. (2021). fv3gfs-wrapper: a python wrapper of the  
 375 fv3gfs atmospheric model. *Geoscientific Model Development*, 14(7), 4401–4409.  
 376 doi: <https://doi.org/10.5194/gmd-14-4401-2021>
- 377 Pan, B., Anderson, G. J., Goncalves, A., Lucas, D. D., Bonfils, C. J. W., Lee, J.,  
 378 ... Ma, H.-Y. (2021). Learning to correct climate projection biases. *Jour-*  
 379 *nal of Advances in Modeling Earth Systems*, 13(10), e2021MS002509. doi:  
 380 <https://doi.org/10.1029/2021MS002509>
- 381 Paszke, A., Gross, S., Massa, F., Lerer, A., Bradbury, J., Chanan, G., ... Chin-  
 382 tala, S. (2019). Pytorch: An imperative style, high-performance deep  
 383 learning library. *CoRR, abs/1912.01703*. doi: <https://doi.org/10.48550/>  
 384 [arXiv.1912.01703](https://doi.org/10.48550/arXiv.1912.01703)
- 385 Putman, W. M., & Lin, S.-J. (2007). Finite-volume transport on various cubed-

- 386 sphere grids. *Journal of Computational Physics*, 227(1), 55 - 78. doi: <https://doi.org/10.1016/j.jcp.2007.07.022>
- 387
- 388 Saha, S., Moorthi, S., Wu, X., Wang, J., Nadiga, S., Tripp, P., ... Becker, E. (2014,  
389 March). The NCEP Climate Forecast System Version 2. *Journal of Climate*,  
390 27(6), 2185–2208. doi: <https://doi.org/10.1175/JCLI-D-12-00823.1>
- 391 Thiébaux, J., Rogers, E., Wang, W., & Katz, B. (2003, May). A New High-  
392 Resolution Blended Real-Time Global Sea Surface Temperature Analy-  
393 sis. *Bulletin of the American Meteorological Society*, 84(5), 645–656. doi:  
394 <https://doi.org/10.1175/BAMS-84-5-645>
- 395 Watt-Meyer, O., Brenowitz, N. D., Clark, S. K., Henn, B., Kwa, A., McGibbon,  
396 J., ... Bretherton, C. S. (2021). Correcting weather and climate models by  
397 machine learning nudged historical simulations. *Geophysical Research Letters*,  
398 48(15), e2021GL092555. doi: <https://doi.org/10.1029/2021GL092555>
- 399 Wehner, M. F., Smith, R. L., Bala, G., & Duffy, P. (2010). The effect of hor-  
400 izontal resolution on simulation of very extreme us precipitation events  
401 in a global atmosphere model. *Climate Dynamics*, 34(2), 241–247. doi:  
402 <https://doi.org/10.1007/s00382-009-0656-y>
- 403 Weyn, J. A., Durran, D. R., & Caruana, R. (2020). Improving data-driven  
404 global weather prediction using deep convolutional neural networks on a  
405 cubed sphere. *Journal of Advances in Modeling Earth Systems*, 12(9),  
406 e2020MS002109. doi: <https://doi.org/10.1029/2020MS002109>
- 407 Zhou, L., Lin, S.-J., Chen, J.-H., Harris, L. M., Chen, X., & Rees, S. L. (2019). To-  
408 ward convective-scale prediction within the next generation global prediction  
409 system. *Bulletin of the American Meteorological Society*, 100(7), 1225 - 1243.  
410 doi: <https://doi.org/10.1175/BAMS-D-17-0246.1>
- 411 Zhu, J., Park, T., Isola, P., & Efros, A. A. (2017). Unpaired image-to-image transla-  
412 tion using cycle-consistent adversarial networks. *CoRR*, *abs/1703.10593*. doi:  
413 <https://doi.org/10.48550/arXiv.1703.10593>